# Experimental study on the unsteady flow between rotors of counter-rotating fan

LI Qiushi*, LI Zhiping and LU Yajun

(Department of Propulsion, Beijing University of Aeronautics and Astronautics, Beijing 100083, China)

Received July 15, 2001; revised September 18, 2001

**Abstract** A more accurate calibration and measurement technique with a single wire velocity measuring instrument is used to study the unsteady velocity between the rotors of a counter-rotating axial fan, and some special concluding remarks of unsteady effects were obtained. The unsteady potential influence of the downstream rotor is a dominant factor; the wake disturbance of the upstream rotor is less important. The radial velocity is mainly affected by the vortex strength of the secondary flow at the upstream blade tip and hub region. These results are important for elucidating the mechanism of unsteady flow in a counter-rotating axial compressing system.

**Keywords:** turbomachinery, unsteady flow, dynamic measuring, wake flow.

The counter-rotating axial compressing system is a new field that scientists worldwide develop and explore eagerly[1]. But to apply this kind of system to an engine has some difficulties to overcome such as structural problem, its unique flow type, the unsteady effect and a series of aerodynamic influence, which make the research limited to steady and low velocity. In the present work the nonlinear optimization of Levenberg-Marguardt[2] method is employed to improve the calibration and experimental technique. Furthermore, the velocity field between the rotors of counter-rotating axial fan is calculated using an improved empirical formula,

$$V_{\text{eff}}/V = A^0 + A^1\cos\theta_y + A^2\sin\theta_y, \quad (1)$$

where $V_{\text{eff}}$ is the effective refrigeration velocity, $V$ the actual flow velocity at probe place, and the coefficient matrix $\boldsymbol{A}^i$ is defined by

$$\begin{aligned}\boldsymbol{A}^i = {} & a_1^i + a_2^i\theta_y + a_3^i\theta_p + a_4^i V + a_5^i\theta_y^2 \\ & + a_6^i\theta_p^2 + a_7^i V^2 + a_8^i\theta_y\theta_p + a_9^i\theta_y V \\ & + a_{10}^i\theta_p V + \cdots. \end{aligned} \quad (2)$$

Here, the coefficients $a_j^i$ are obtained using the least square fitting for the calibration data of the single wire. In fairly wide flow angle range, a very good precision can be obtained when Eq. (2) is taken divalent. On the other hand, for eliminating the random error, six deflection angles are chosen to get the three-dimensional velocity vector presented by the velocity magnitude $\boldsymbol{V}$, the horizontal deflection $\beta$ and the pitch angle $\theta_p$. Therefore it becomes possible to handle the above-mentioned experimental data and to solve the problem of a nonlinear least square, in the same way as to make the goal function $Q = \sum_{i=1}^{n}[y_i - f(V, \beta - m_i, \theta_p, a)]^2$ minimum, where $a$ is the coefficient set in Eq. (2), which can be determined according to the calibration.

To check the above-mentioned method with the calibration data, the velocity error is controlled within 1 m/s, the angle error within 1°. Figs. 1 and 2 show the tested calibration curve of the hot wire.

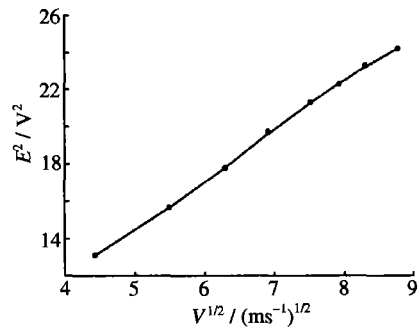


Fig. 1. The voltage-velocity linearized curve of the instrument.

To eliminate the influence of temperature change in the process of calibration and measurement, a temperature revised formula[3] is adopted, $E_r = E\left(\frac{T_s - T_r}{T_s - T}\right)^{1/2}$, where $T_s$ is the working temperature of the hot wire, defined at 250 ℃ by the TSI company, and $T_r$ the corrected temperature, which is measured to be 29 ℃ in calibration.

* To whom correspondence should be addressed. E-mail: lqs@ns.ngl.buaa.edu.cn

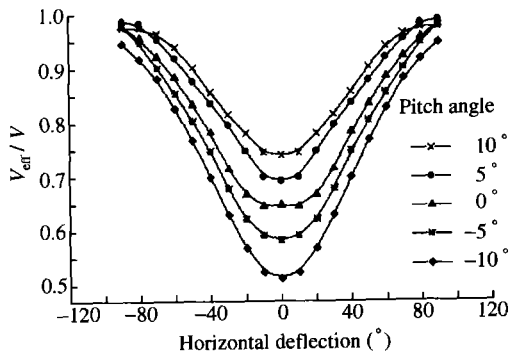


Fig. 2. The calibration curve of the 25.744 m/s.

## 1 Experimental arrangement

The arrangement of the experimental facilities with counter-rotating fan is shown in Fig. 3. The parameters and performance are: the flow rate 11817 $m^3/h$, the total pressure rise 1320 Pa, the impellers' external diameter 450 mm, the hub-tip ratio 0.4889, the generators' nominal rotating speed 2900 r/min, the front generator power 2.2 kW, the rear generator power 3.0 kW, 7 front blades, 8 rear blades, the ratio of aerodynamic loading of front to rear rotor 0.733:1, the number of supporting rods for both front and rear generators is 3 ( with 120° difference).

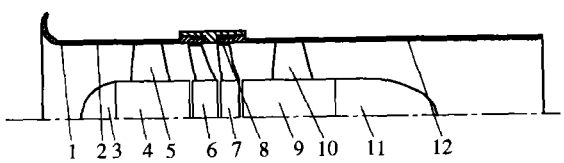


Fig. 3. Structure of the counter-rotating axial fan for experiment. 1, flow gathering ware; 2, front casing; 3, inlet cover; 4, front generator; 5, generator supporting rod; 6, front rotor; 7, rear rotor; 8, intermediate casing; 9, rear generator; 10, supporting rod; 11, outlet valve; 12, rear casing.

Test apparatuses used are: the hot wire velocity instrument 1050 ( including calibration equipment TSI1125X) from TSI company, the magnetic tape TEACSR-51 C portable data recorder with speed of 9.5 m/s and frequency of 2500 Hz, the traverse actuator ROTADATA RTM100A S/N20 (UK), the frequency converter SVF-552-380C, and the Honeywell electromagnetic data-acquisitor KHO-01DB with a responding frequency of 5 kHz. The data collecting system consists of a high speed data collecting board and a PII350 computer sampling at 12 μs intervals and repeating 900 ~ 1000 times under the control of program.

The measuring radial and axial locations of probes are shown in Table 1.

Table 1. Probe locations of measuring points

| Measuring points | 1 | 2 | 3 | 4 | 5 | 6 | 7 |
|---|---|---|---|---|---|---|---|
| Radial position ϕ(mm) | 440 | 420 | 400 | 380 | 360 | 340 | 320 |
| Relative height (%)[a] | 95.65 | 86.96 | 78.26 | 69.57 | 60.87 | 52.17 | 43.48 |
| Chord length[b] | 0.4 | — | — | — | — | — | 0.0625 |
| Chord length[c] | 0.25 | — | — | — | — | — | — |

a) the percentage of the height from the measuring points to the hub compared to the blade's height; b) the distance away from front blade's trailing edge compared to the front blade chord length; c) the distance away from rear blade's leading edge compared to the front blade chord length.

## 2 Analysis of frequency spectra between counter-rotating rotors

The frequency spectra at ϕ440, ϕ380 and ϕ320 measuring points when the rotating speed ratio matches 1:1 are shown in Fig. 4.

Comparing the amplitude of the front blade pulse signals with those of the rear ones, the rear blade potential influence is nearly 4 times greater than the front blade wake disturbing influence. For further study, a frequency converter is employed to change the rotating speed of the front or rear rotors. Firstly, the front rotating speed is changed to 1980 r/min and the rear one to 2882 r/min. The frequency spectra, with the obvious frequencies and corresponding amplitudes of peaks, at ϕ440, ϕ380 and ϕ320 measuring points, are listed in Table 2.

Table 2. Frequency spectra with front speed changed

| Radial location | Front blade pulse signal | | Rear blade pulse signal | | Front pulse signal diploid frequency | |
|---|---|---|---|---|---|---|
| | Fr.(Hz) | Amp. (V) | Fr.(Hz) | Amp. (V) | Fr.(Hz) | Amp. (V) |
| ϕ440 | 229 | 0.0018 | 385 | 0.0067 | 460 | 0.0014 |
| ϕ380 | 230 | 0.0035 | 387 | 0.0067 | 461 | 0.0019 |
| ϕ320 | 231 | 0.0068 | 387 | 0.0093 | 462 | 0.0009 |

To compare with the designed condition of normal rotating speed, the most obvious change is that the influence of the front blade wake disturbance is strengthened. It can be seen that at ϕ320 measuring point, which is only 5 mm away from the front blade trailing edge, the ratio of front blade wake disturbing influence to the rear blade potential influence exceeds 2/3, while it is 1/4 at the blade tip. In fact, the changed front rotating speed could change the flow field condition. At lower rotating speed, separation might occur on the pressure surface, thus the macro-separation might be more evident than the wake disturbance under designed condition. Whereas, the result of analysis shows that the rear blade potential influence is the dominant unsteady source between counter-rotating rotors.

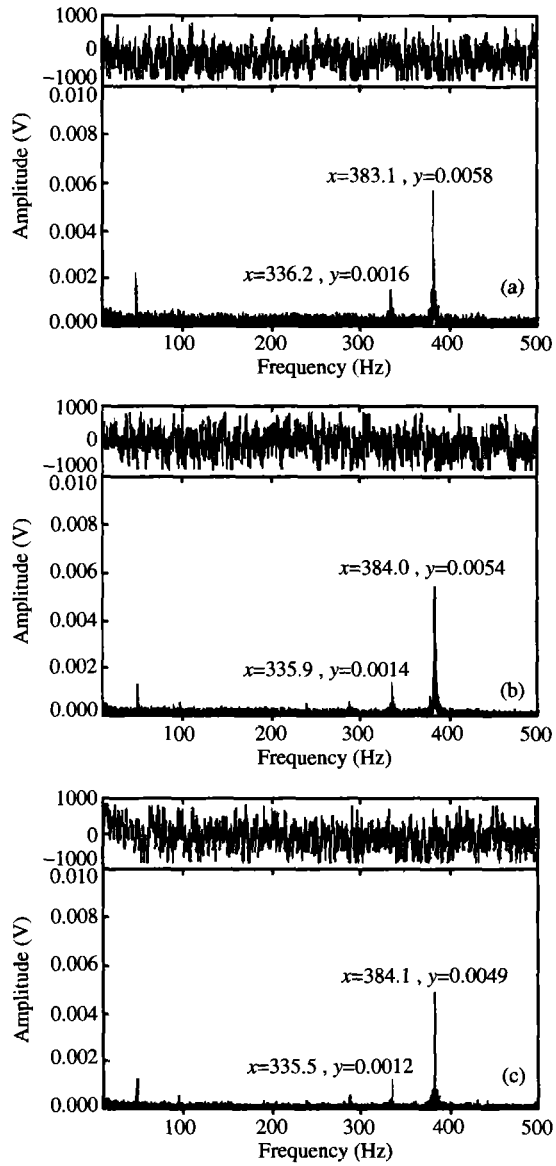


Fig. 4. Frequency spectra at three measuring points. (a) $\phi$440 (blade tip), (b) $\phi$380, (c) $\phi$320 (middle of blade).

When the rear rotating speed was set to 1980 r/min and the front turned back to 2882 r/min, the frequency spectra, with the major frequencies and corresponding amplitudes, are shown in Table 3.

Table 3. Frequency spectra with rear speed changed

| Radial location | Rear blade pulse signal | | Front blade pulse signal | |
|---|---|---|---|---|
| | Fr. (Hz) | Amp. (V) | Fr. (Hz) | Amp. (V) |
| $\phi$440 | 263 | 0.0080 | 334 | 0.0026 |
| $\phi$380 | 264 | 0.0087 | 334 | 0.0013 |
| $\phi$320 | 263 | 0.0058 | 335 | 0.0009 |

It is obvious that the rear blade potential influence is continuously acting as the leading role in the unsteady flow field between the two rotors. Even at the $\phi$320 measuring point, which is very near to the front blade trailing edge, the front blade wake disturbance is less than 1/6 of the rear blade potential influence.

Through the analysis of frequency spectra, it can be concluded that in the flow field between the two counter-rotating rotors, the rear blade potential influence is stronger than the front blade wake disturbance. Therefore, an average method of phase locking on both the front and the rear rotors instead of on the front rotor only was employed in this study. If it is restricted by the number of sampling which should be at least 150 ~ 200 samples being averaged, the phase locking on the rear rotor only might be a good substitution because the influence of front blade is considered comparatively small. The reason for this phenomenon may be the high converse pressure gradient produced by the high loading on the rear blade relative to that on the front.

## 3 Analysis of unsteady velocity contour between counter-rotating rotors

The velocity distribution (shown in Fig. 5) in 8 regions of mainstream and non-mainstream shows that the influence of the rear rotor takes the dominant position in the field between the rotors. On the other hand, because the number of front blades is 7, the mainstream is strengthened at the site where two rotors overlapped, but it is stretched and weakened where the mainstream region of rear rotor encounters the non-mainstream region of front rotor because of the inverse phase.

Attention should be focused on the radial velocity distribution contours. The air flow lumps towards external diameter are distributed evenly in 7 directions, showing the property of the front rotor. It means that in the axial and tangent directions, the influence of rear rotor plays the leading role, but in radial direction, the influence of the front rotor is the dominant. The main reason for that might be the clearance vortex and the passage vortex in the region of front blade tip and hub. These results show that the potential influence of rear rotor affects the flow mainly on cylinder surface, rather than the radial direction. Since the front blades had been skewed forward severely, it made the passage vortex displaced away from the trailing edge by mainstream rapidly, and made the three-dimensional velocity field between the two rotors more complicated. Especially, because the aero-

dynamic design for the front blade adopted the exponential loading rule, which allocated the most loading on the tip, the effect of secondary flow produced by clearance and end wall was severe. So the strength of clearance vortex was larger than that under common condition, and the flow was also separated much more. Therefore, the radial velocity field between counter-rotating rotors exhibited the frequency characteristic of the front rotor.

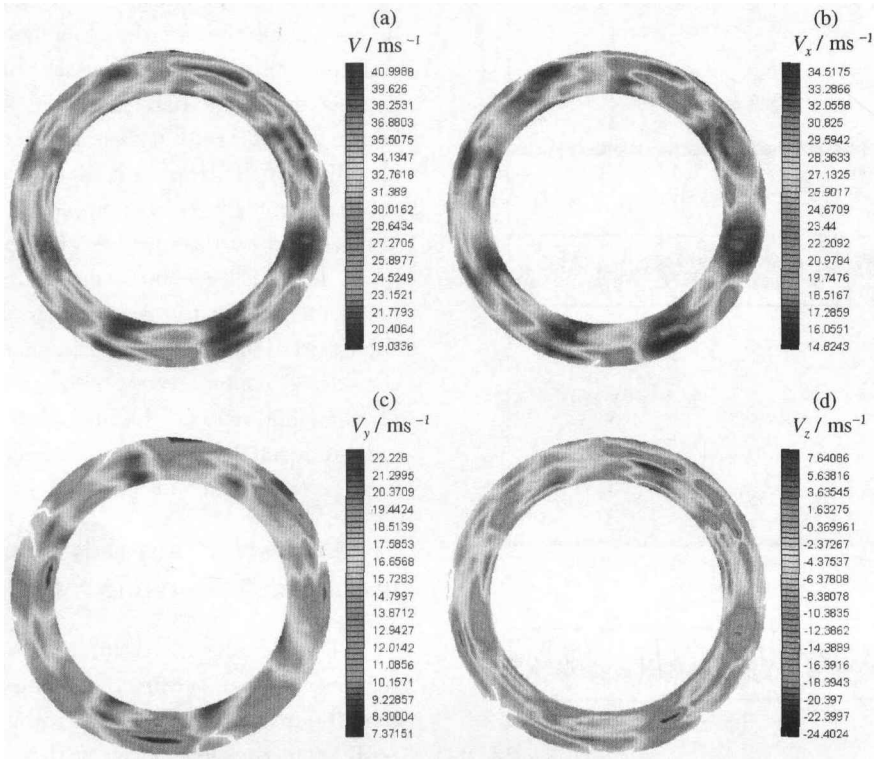


Fig. 5. Velocity distribution cloud contour of the total velocity (a), axial velocity (b), tangent velocity (c) and radial velocity (d).

Fig. 6 shows the fluctuations of the axial and tangential velocities at the 95.65% relative blade height. Because the influence number of the front rotor is 7 and that of the rear is 8 in each of their complete rotating period, the fluctuation period of velocity is different from one another. Theoretically, under the constant rotating speed of both rotors, the pulses of velocity would coincide after the two rotors had completed one rotating period. Besides, during the sampling time of 10 ms, either the axial velocity fluctuation or the tangential one had gone through 4 periods, in other words, they would go through 8 periods in a rotating period of 20 ms, which reflects the passing through frequency characteristic of the rear rotor.

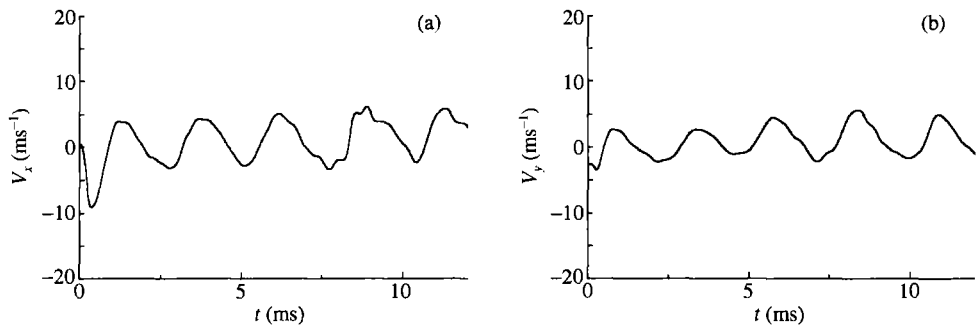


Fig. 6. Axial velocity pulse (a), tangential velocity pulse (b) at the 95.65% relative blade height.

At the 86.96% and 43.48% relative blade heights, the velocity fluctuations were basically consistent to that at 95.65%, with a little discrepancy on amplitude and phase only. Hereby, these above-mentioned test parameters also reflect the disturbing flow field between counter-rotating rotors dominated

mainly by the pressure wave of rear blade spreading forward.

## 4 Concluding remarks

For the typical output characteristics of the single wire velocity-measuring instrument, a nonlinear optimization Levenberg-Marguardt algorithm was adopted. Furthermore, with the aid of traverse actuator, high-speed data collecting system and the sampling average technology of phase locking on both rotors, the three-dimensional unsteady velocity between counter-rotating rotors has been measured accurately.

(i) The unsteady potential influence, mainly the downstream pressure wave of rear blade spreading forward, plays the leading role in the whole unsteady periodic influence, while the upstream wake disturbing influence is less important. The main reason lies in the high converse pressure gradient of the rear rotor.

(ii) The potential influence of downstream rotor plays the leading role mainly on $S_1$ flow surface, but for the radial velocity, it is related to the vortex strength of the secondary flow produced by the front blade tip and hub region. Therefore, the key to further improving the performance of fan /compressor system is to reduce the loading of these two regions under the condition that the total loading is ensured[1)].

## References

1 Sharma, P. B. et al. A review of recent research on contra-rotating axial flow compressor stage. International Gas Turbine and Aeroengine Conference, Birmingham, UK, 1996, 96-GT-254.
2 Li, C. et al. The calibration method of the velocity and direction characteristics of single hot wire. J. Gansu Industrial University (in Chinese), 1997, 23(2): 42.
3 Sheng, S.Z. et al. An Introduction to the Hot Wire Velocity Instrument (in Chinese), Beijing: Beijing University Press, 1987, 60～71.

1) Li, Q. S. Numerical simulation and experimental study for counter-raotating axial compressor, Ph.D. Dissertation, Beijing University of Aeronautics and Astronautics, 2000.